Electrosynthesis of hierarchical Cu2O–Cu(OH)2 nanodendrites supported on carbon nanofibers/poly(para-phenylenediamine) nanocomposite as high-efficiency catalysts for methanol electrooxidation

El Mahdi Halim, Hubert Perrot, Ozlem Sel, Catherine Debiemme-Chouvy, Khalid Lafdi, Mama El Rhazi

Electrosynthesis of hierarchical Cu_2O-$Cu(OH)_2$ dendrites supported on carbon nanofibers/poly(*para*-phenylenediamine) nanocomposite as high-efficiency catalysts for methanol electrooxidation

El Mahdi Halim [*,†,‡], *Hubert Perrot* [‡], *Ozlem Sel* [‡], *Catherine Debiemme-Chouvy* [‡], *Khalid Lafdi* [§], *Mama El Rhazi* [†]

[†] *University of Hassan II of Casablanca, Faculty of Sciences and Technology, Laboratory of Materials, Membranes and Environment -BP 146, 20650 Mohammedia, Morocco*

[‡] *Sorbonne Université, CNRS, Laboratoire Interfaces et Systèmes Electrochimiques, LISE, 75005 Paris, France*

[§] *University of Dayton, Department of Chemical and Materials Engineering, 45440, Ohio, USA*

*** Corresponding authors: Email:** elmahdi.halim@gmail.com

ABSTRACT

The development of highly efficient catalysts using inexpensive and earth-abundant metals is a crucial factor in a large-scale commercialization of direct methanol fuel cells (DMFCs). In this study, we explored a new catalyst based on copper dendrites supported on carbon nanofibers/poly(*para*-phenylenediamine) (CNF/P*p*PD) nanocomposite for methanol oxidation reaction (MOR). The catalyst support was prepared on a carbon paste electrode using electropolymerization of *para*-phenylenediamine monomer on a drop-cast carbon nanofibers network. Afterwards, the copper dendrites (CuDs) were electrodeposited on the nanocomposite through a potentiostatic method. The morphology and the structure of the prepared nanomaterials were characterized by a transmission electron microscope, scanning electron microscope, energy dispersive X-ray, X-ray diffraction, and an X-ray photoelectron spectroscope. The results suggested that a three-dimensional dendritic structure consisting of Cu_2O and $Cu(OH)_2$ formed on the hybrid CNF/P*p*PD nanocomposite. The catalytic performance of copper dendrites supported on CNF, P*p*PD and CNF/P*p*PD catalyst supports was evaluated for MOR under alkaline conditions. The CNF/P*p*PD/CuDs exhibits a highest activity (50 $mA.cm^{-2}$) and stability toward MOR over 6h, with respect to CNF/CuDs (40 $mA.cm^{-2}$) and P*p*PD/CuDs (36 $mA.cm^{-2}$). This inexpensive catalyst with high catalytic activity and stability is a promising anode catalyst for alkaline DMFC applications.

KEYWORDS: methanol electrooxidation; electrocatalysis; copper dendrites; carbon nanofibers; poly(*para*-phenylenediamine).

1. INTRODUCTION

The massive growth of population around the world accompanied by the tremendous industrial development, as well as the environmental consequences caused by oil, have led to growing demand for new and effective energy sources [1–3]. However, when addressing energy issues and meeting the world's energy needs, it is extremely important to consider the serious consequences of this development on the environment, especially the problem of global warming [4,5]. Fuel cell has been considered as a promising candidate to get over the current and future problems of energy. Especially, direct methanol fuel cells (DMFCs) present a remarkable advantage over the other types of fuel cells, such as their excellent volumetric energy density, high operating efficiency and ease of transportation/storage and large availability of methanol. Therefore, DMFCs are widely considered for their potential application in potable mobile devices and in automobile fields [6,7].

DMFC-anode electrocatalysts based on platinum have been extensively studied, because of their high catalytic properties to enhance the efficiency of methanol oxidation reaction (MOR) [8–11]. However, some limitations still obstruct the wide-scale commercialization of DMFCs, namely, the high cost of platinum and the poisoning of the electrocatalyst surface by the formation of the intermediate CO species during MOR. Consequently, several studies have been conducted and much efforts are underway to prepare electrocatalysts using inexpensive and earth-abundant metals with high electrocatalytic performance. Copper-based catalyst has received considerable attention due to its promising regarded performance for MOR and its lower affinity to CO species compared

to noble metals [12,13] even though its low to moderate stability [14]. Therefore, the association of copper with other metals [12,15–17] or the use of copper (hydro)oxide structures [14,18,19] could be suitable ways to overcome the stability problem. Cuprous oxide (Cu_2O) is a p-type semiconductor, which was considered as an attractive and promising catalyst thanks to its band gap (2.0-2.2 eV) [20–22]. Ashassi-Sorkhabi *et al.* prepared a catalyst based on polypyrrole (PPy) electrochemically doped by cuprous oxide (Cu_2O), gold nanoparticles (Au) and nanodiamond (ND) for methanol electrooxidation. The results showed that Cu_2O manifested a good catalytic activity for MOR, while PPy, ND, and Au acted as catalyst-support to promote its catalytic performance [23]. Other studies demonstrated that the morphology of the deposited copper catalyst plays an important role in enhancing catalytic performance by increasing the real surface area and enlarging the available electrochemical active sites [24,25]. In this context, CuO and $Cu(OH)_2$ nanowires were prepared by Pawar *et al.* through a chemical oxidation. The nanowires exhibited high electrocatalytic activity for methanol oxidation with a current density of about 50 $A.g^{-1}$. The good catalytic performance of this catalyst was related to the electroactive nanostructure formed, which leads to facilitate the electron transfer at the surface of the electrode and to increase the electrochemical active sites [26]. Chen *et al.* reported the synthesis of three-dimensional nanoporous copper catalyst and provided that the high porosity and the large specific surface area of the catalyst were key factors for a high catalytic effect [25]. In another work, Chang *et al.* compared nanodendrites and nanowires of Pt-Pd-Cu hierarchical morphologies in which, copper metal was used for improving CO_{ads} tolerance and ensuring a high utilization of Pt by creating tip-cracked defects. The nanodendrite morphology of Pt-Pd-Cu catalyst showed an improved electrocatalytic activity and stability for methanol oxidation with respect to the nanowire morphology [27].

Regarding the effect of the catalyst support, multiple roles have been discussed, for instance: (i) increasing the stability of the catalyst, (ii) offering a high active surface area for the deposited catalyst, (iii) contribution in the mass transfer and the oxidation reaction and (iv) reducing the poisoning of the catalyst surface. Moreover, it can increase the number of the catalytic site and improve their intrinsic activity [28–30]. Due to both high electronic conductivity and high surface area offered, carbon materials are the most commonly used catalyst supports [12,20,31,32]. Carbon nanofibers-supported catalyst exhibited enhanced catalytic performance than other carbon-supports thanks to their unique structure combining chemical and physical properties. Calderon *et al.* studied the performance of Pt-Ru supported on CNFs as anode material for DMFC. The results showed that Pt-Ru/CNF revealed a higher catalytic performance compared to the commercial Pt-Ru/C catalyst, and the CNF improved the CO tolerance during MOR [33]. In another work, Mu *et al.* discussed the possible use of graphene-embedded carbon fiber as support for Pt nanoparticles (PtNPs) for both methanol oxidation and oxygen reduction reactions. Promising electrochemical properties were obtained, which were attributed to the fact that graphene-embedded carbon fiber (RGO/CF) support offers abundant graphitic-N and oxygen functions for a good dispersion of active Pt NPs and promotes their catalytic performance [34]. Accordingly, carbon support plays an important role in enhancing the dispersion and the performance of the catalyst by providing an underlying framework for facile electron conduction. However, carbon support suffers from corrosion and dissolution, which decrease its stability. Lately, the hybrid conducting polymer-carbon materials have been considered as novel promising support with special properties that cannot be attained by the individual components [29]. The deposition of conducting polymer (CP) on carbon support improves the electrochemical and mechanical stability of the catalyst and could exhibit a good

tolerance to CO poisoning during the methanol electrooxidation [30,35,36]. Poly(*para*-phenylenediamine) (P*p*PD) is an aromatic CP that provides a large number of amine groups. The latter can improve the deposition conditions of the catalyst and thus, its electronic properties for higher catalytic performance [37,38]. P*p*PD has been used to functionalize CNTs and rGO supports [39,40]. It has been demonstrated that the carbon-P*p*PD nanocomposites were formed by the π-π stacking interaction, providing helpful supports for an effective attachment and dispersion of catalyst nanoparticles. Besides, P*p*PD prevents the agglomeration and the migration of nanoparticles by coordination with the amine groups.

In this study, a new, inexpensive and effective anode material based on copper dendrites (CuDs) supported on carbon nanofibers/poly(*para*-phenylenediamine) (CNF/P*p*PD) nanocomposite is reported. CNF/P*p*PD was formed by a dispersion of CNFs on carbon paste electrode followed by an electropolymerization of P*p*PD. Then, CuDs were prepared on CNF/P*p*PD nanocomposite through a potentiostatic method. The morphological and compositional characterizations of the electrodes was analyzed by TEM, FEG-SEM, EDX, XRD and XPS methods. In order to investigate the optimized CNF/P*p*PD/CuDs composition, the effect of different constituents on the electrochemical properties of the nanocomposite were evaluated by CV and EIS. The results show that the CuDs consist of Cu_2O and $Cu(OH)_2$ phases. Further, the catalytic performance of CNF/P*p*PD/CuDs for MOR and the effect of the CNF/P*p*PD support were evaluated in alkaline media. The results of the present work revealed that CNF/P*p*PD/CuDs nanocomposite presents a high electrocatalytic activity and stability, which could increase its potential use as a promising anode material for alkaline DMFCs and other electrochemical systems.

2. EXPERIMENTAL PART

2.1. Materials

Carbon nanofibers were synthesised at Applied Sciences Inc. and were from the Pyrograf III family. Graphite powder (<20 μm; synthetic 100 %), *para*-phenylenediamine monomer (*p*PD) (1,4-diaminobenzene), mineral oil heavy, copper chloride ($CuCl_2$; 99.99 wt %), sodium hydroxide (NaOH; ≥ 98 %), sodium sulfate (Na_2SO_4; ≥ 99 %), potassium ferrocyanide-ferricyanide ($K_3Fe(CN)_6/K_4Fe(CN)_6.3H_2O$; ≥ 99 %), potassium chloride (KCl; 99 %), methanol (MeOH; 99.8 wt %), sulfuric acid (H_2SO_4; 98 wt %), nitric acid (HNO_3; 70 wt %), and dimethylformamide (DMF; 99.5 %) were purchased from Sigma-Aldrich.

2.2. Preparation of the CNF/PpPD catalyst support

CNFs were initially treated with a mixture of sulfuric and nitric acids to create carboxylic (-COOH), carbonyl (-CO), and hydroxyl (-COH) groups on the surface according to reported work [38]. After the dispersion of the functionalized CNFs in DMF (2 mg CNF in 1 mL DMF) by ultrasonic treatment, 10 μL portion of the prepared dispersion was drop-cast on the surface of carbon paste electrode (CPE with diameter of about 3 mm) and dried for 10 min at 80 °C, this electrode is called CNF modified electrode. The preparation of P*p*PD film was performed on CNF modified electrode using three-electrode configuration, in which, a CNF modified electrode as working electrode, a saturated calomel electrode (SCE) as reference electrode, and a platinum rod as counter electrode were used. The CNF modified electrode was immersed in a 0.1 M of sulfuric acid solution containing 5 mM of *p*PD monomer, then the P*p*PD film was produced by cyclic voltammetry (CV) for 10 cycles

between -0.1 V and 0.9 V at 50 mV s^{-1} **(Fig. 1)**. CNF and P*p*PD were also prepared separately on CPE using the same process described above to evaluate the reactivity of the individual component.

2.3. Preparation of dendritic copper electrocatalyst on CNF, PpPD, and CNF/PpPD supports

Dendritic copper (CuDs) electrocatalyst was electrodeposited on CNF, P*p*PD, and CNF/P*p*PD modified electrodes by applying a fixed potential of -0.5 V *vs. SCE* for 45 s, unless otherwise stated, in a 0.1 M of Na_2SO_4 solution containing 0.1 M $CuCl_2$ using three-electrode configuration. **Fig. 1** presents the synthesis strategy of the CNF/P*p*PD/CuDs nanocomposite on CPE electrode.

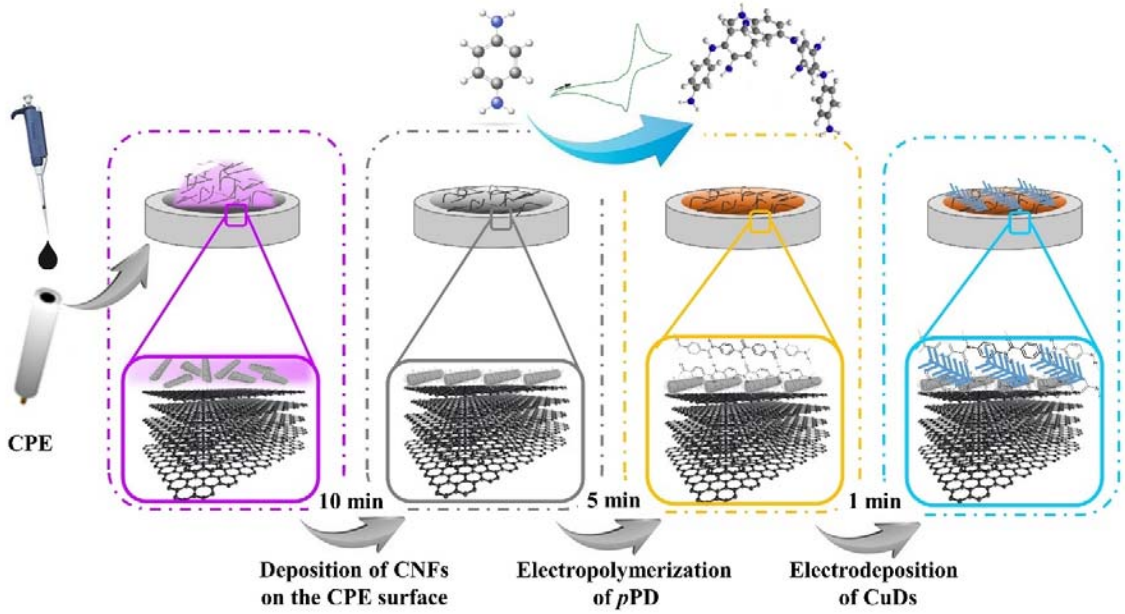

Fig. 1. *Schematic description of the fabrication strategy of CNF/PpPD/CuDs on CPE.*

2.4. Morphological and structural characterizations

The surface morphology and composition of the modified electrodes were investigated by a field emission gun scanning electron microscope (FEG-SEM, Zeiss, Supra 55), transmission electron

microscopy (TEM, JEOL, JEM-1011 electron microscope), and energy dispersive X-ray spectrometer (EDX). X-ray photoelectron spectroscopy (XPS) analyses were performed using a K-alpha spectrometer (Thermo Scientific) equipped with a monochromatized Al anode (1486.6 eV) and using a pass energy of 100 eV and 20 eV, for acquisition of the survey and high-resolution spectra, respectively. The atomic concentration of the surface (≈ 10 nm) of the samples was calculated after subtraction of the background using Shirley method [41]. X-ray diffraction (XRD) measurements were performed by a Panalytical Empyrean diffractometer equipped with a Cu-Kα as a radiation source (Kα = 1.54 □).

2.5. Electrochemical measurements

Cyclic voltammetry (CV), electrochemical impedance spectroscopy (EIS) and chronoamperometry measurements were carried out using a three-electrode configuration, in which a saturated calomel electrode (SCE) was used as a reference electrode, a modified CPE was used as a working electrode, and a platinum (Pt) rod as a counter electrode. The electrochemical explorations were performed by PalmSens electrochemical interface, controlled with PSTrace software (version 4.6). All experiments were carried out at room temperature.

3. RESULTS AND DISCUSSION

3.1. Preparation of CNF/PpPD/CuDs on carbon paste electrode

3.1.1. pPD preparation

Fig. 2. (a) and **(b)** show the 1st and the 10th cycles of the electropolymerization of *p*PD, respectively. The results obtained on two types of substrates are shown here, *i.e.* CPE and CPE previously

modified with CNFs. The voltammograms of both electrodes display the presence of two redox peaks, the first redox peak is attributed to the oxidation and the reduction of *p*PD monomer, and the second redox peak corresponds to the electrochemical behaviour of the electroactive P*p*PD film [42–44]. The electrochemical parameters of both redox peaks are reported in **Table SI.1**. Contrary to the current of the first redox peak, that of the second one increases during cycling, indicating the formation of a thin electroactive film on the electrode surface. The electropolymerization of *p*PD on CNF modified electrode presents a higher current density and reduced peak-to-peak potential separation values compared to CPE, which could be explained by the high surface area and the enhanced electrical properties of CNFs [45].

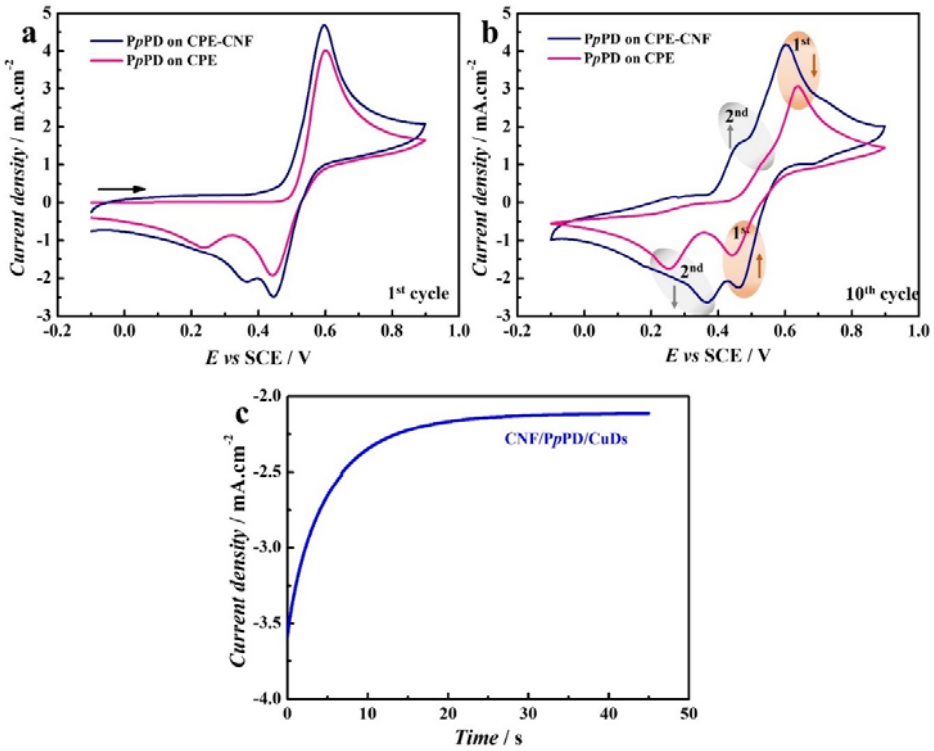

Fig. 2. *Cyclic voltammograms of the 1st cycle (a) and the 10th cycle (b) of the electropolymerization of pPD on the CPE and on the CPE-CNF in 0.1 M H_2SO_4 containing 5 mM of pPD monomer for 10 cycles, at a scan*

rate of ν=50 mV s^{-1}, and chronoamperometric curve of the electrodeposition of CuDs on CNF/PpPD electrode at a fixed potential of -0.5 V for 45 s in 0.1M Na_2SO_4 containing 0.1 M $CuCl_2$ (c).

3.1.2. CuDs electrogeneration

After the formation of the P*p*PD film on CNFs, CuDs were electrodeposited on the modified electrode through potentiostatic method at a potential of -0.5 V *vs. SCE* for 45 s. **Fig. 2. (c)** shows the electrodeposition curve of CuDs on CNF/P*p*PD nanocomposite. In the beginning, the current decreases rapidly due to a fast nucleation-growth process [46,47]. After 30 s, the current density stabilizes at about -2.12 mA.cm^{-2}, which could be related to the depletion of the copper ion concentration near to the electrode surface [46].

3.2. Morphological and structural characterizations

3.2.1. FEG-SEM, TEM and EDX analyses

The FEG-SEM image of CNF/P*p*PD **(Fig. 3. (a))** shows that the CNFs with an average diameter of about 150 nm, were uniformly dispersed on the electrode surface forming a CNF network, which offered a larger surface area compared to that of the bare CPE **(see Fig. SI.1)** [44]. Moreover, the image displays a very thin-film of P*p*PD polymer deposited on CNFs network which connected all the nanofibers [38]. TEM image of CNF/P*p*PD nanocomposite **(Fig. 3. (b))** shows that CNFs present a smooth surface and a uniform deposition of thin polymer film on the CNFs, in agreement with the FEG-SEM image in **Fig. 3. (a)**. Regarding the morphology of CNF/P*p*PD/CuDs, FEG-SEM image **(Fig. 3. (c))** shows the formation of a three-dimensional copper dendritic structure on CNF/P*p*PD nanocomposite. The deposited copper dendrites present a hierarchical structure

constituted by multiple symmetrical branches attached to a pronounced central backbone. TEM image of the ternary nanocomposite **(Fig. 3. (d))** confirms the formation of a three-dimensional copper dendritic structure on CNF/P*p*PD nanocomposite support.

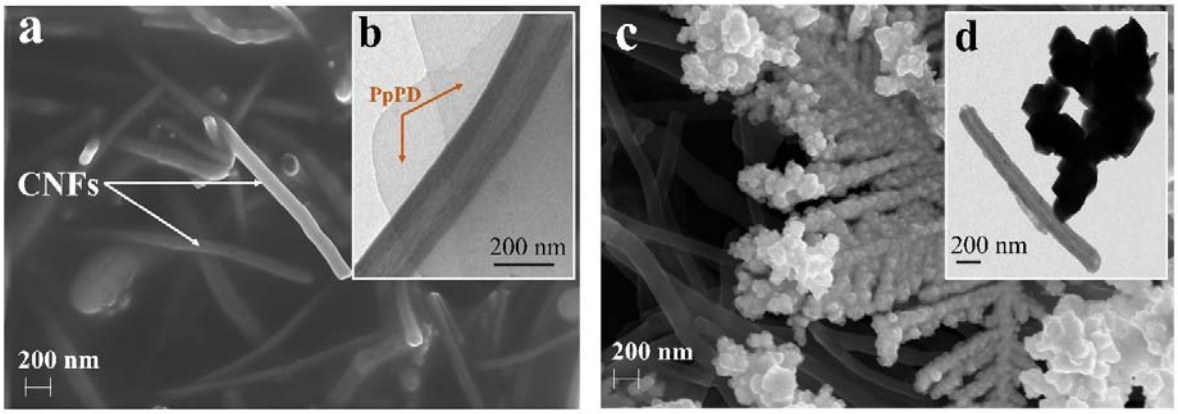

Fig. 3. *FEG-SEM image of CNF/PpPD (a), TEM image of CNF/PpPD (b), FEG-SEM image of CNF/PpPD/CuDs (c), and TEM image of CNF/PpPD/CuDs (d).*

The surface composition of CNF/P*p*PD/CuDs electrode was analysed by Energy-dispersive X-ray (EDX) detector coupled to FEG-SEM. EDX spectrum depicted in **Fig. 4. (a)** demonstrates the presence of N, O, C and Cu elements. N element is related to the P*p*PD polymer, whereas C and O principally originate from CNFs. The EDX mapping was performed to study the elemental distribution on the surface of CNF/P*p*PD/CuDs electrode. As shown in **Fig. 4. (b),** carbon and oxygen elements display a distribution related to CNFs. The nitrogen shows a good distribution on the surface which certifies the formation of P*p*PD thin film on the CNFs. In addition, oxygen has a similar distribution as copper, indicating the formation of a copper oxide and/or copper hydroxide phases. The distribution of nitrogen presents similar areas to the that of copper. This observation confirms that the presence of amine groups offered by P*p*PD polymer, on the surface, facilitates the

nucleation and growth of the copper dendrites, which could improve their electrocatalytic performance [39,48–51]. In order to determine the crystalline structure of the deposited CuDs and surface composition of the resulting films, further characterization was performed by XRD and XPS analyses, respectively.

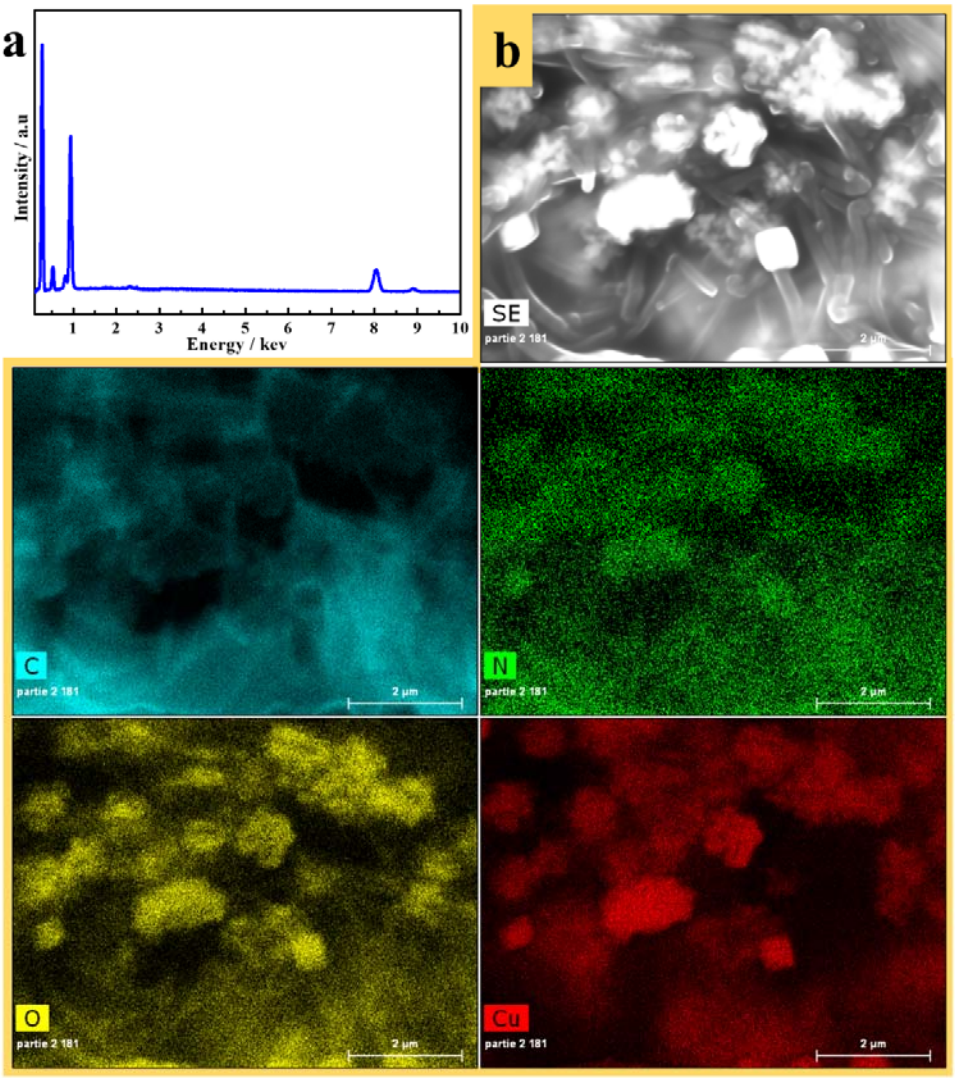

Fig. 4. *EDX spectrum of CNF/PpPD/CuDs (a), Elemental mapping analysis of CNF/PpPD/CuDs* (b).

3.2.2. XRD and XPS analyses

The X-ray diffraction (XRD) was used to characterize the crystalline phase of CNF/P*p*PD/CuDs nanocomposite deposited on CPE as reported in **Fig. 5. (a)**. The XRD pattern shows the presence of two crystalline phases of copper. The diffraction peaks at 16.7°, 23.8°, 39.8°, 47°, 53.2°, 77.7°, and 83.5° correspond respectively to the (022), (021), (130), (112), (150), (153), and (242) planes of $Cu(OH)_2$, which match well to the orthorhombic $Cu(OH)_2$ (JCPDS 01-072-0140) [52]. The peaks appearing at 36.4°, 42.3°, 61.3°, and 73.5° are related to (111), (200), (220), and (311) planes of the cubic Cu_2O (JCPDS 01-077-0199) [53]. In addition, the XRD spectrum shows the presence of a peak at 2θ=26° attributed to the hexagonal structure of the CNFs and the crystalline peaks of CPE substrate.

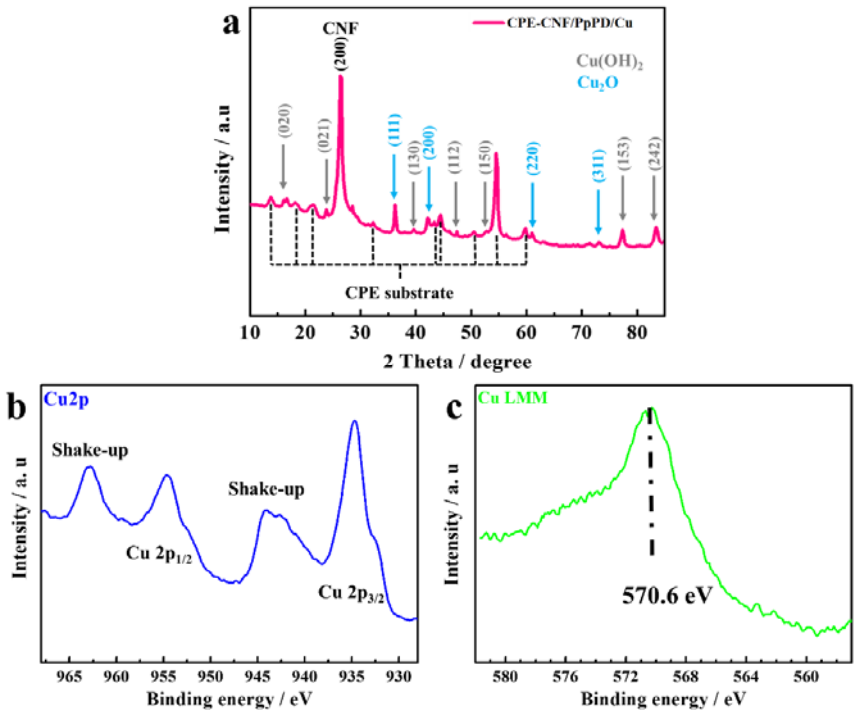

Fig. 5. *XRD pattern (a), XPS high-resolution Cu 2p spectrum (b), and high-resolution Cu LMM spectrum (b) of CNF/P*p*PD/CuDs deposited on CPE substrate.*

Further characterization by X-ray photoelectron spectroscopy (XPS) was investigated to analyze the chemical composition and the state of nanocrystal of the CNF/P*p*PD/CuDs nanocomposite surface within ≈ 10 nm. The surface chemical composition of the nanocomposite was determined, the presence of C, N, O, and Cu elements was detected with an atomic percentage of 62.65, 4.8, 25.6, and 6.95, respectively.

Fig. 5. (b) presents the high-resolution spectrum of Cu2p level. This spectrum is resolved into several peaks: two peaks at around 934.7 eV and 954.5 eV ascribed to $Cu2p_{3/2}$ and $Cu2p_{1/2}$, respectively, which are related to Cu(II) in $Cu(OH)_2$. Additionally, the shake-up satellite peaks at around 942.2 eV and 962.7 eV for Cu $2p_{3/2}$ and Cu $2p_{1/2}$, respectively, indicate the presence of an unfilled $Cu3d^9$ shell, which confirm the existence of Cu(II) at the nanocomposite surface [54,55]. The two contributions situated at 932.4 and 952.5 eV correspond to $Cu2p_{3/2}$ and $Cu2p_{1/2}$, respectively, which are corresponded to Cu(I) or Cu(0). The shape of the Cu LMM Auger peak (**Fig. 5. (c)**) and its location at 570.6 eV, are characteristic of the presence of Cu(I) [56]. Finally, the low intensity of the contribution due to Cu_2O and the high intensity of the one due to $Cu(OH)_2$ could indicate the formation of a thin protection layer of $Cu(OH)_2$ on Cu_2O [54].

3.3. Electrochemical characterizations

Electrochemical characterizations were conducted to evaluate the effect of each component on the electrochemical properties of the CNF/P*p*PD/CuDs modified electrode. Therefore, CVs of bare CPE, CNF, P*p*PD, CNF/P*p*PD, and CNF/P*p*PD/CuDs electrodes were recorded in 0.1 M KCl solution containing 5 mM of $Fe(CN)_6^{3-}/Fe(CN)_6^{4-}$. As shown in **Fig. 6. (a)**, CV curves of the four electrodes present a pair of redox peak corresponding to the reversible reaction of $Fe(CN)_6^{3-}$

/$Fe(CN)_6^{4-}$. The electrochemical parameters of different electrodes recorded from CV curves (**Fig. 6. (a)**) are reported in **Table SI.2**. The bare CPE shows a small redox peak and a high peak-to-peak potential separation (ΔE_p) of about 580 mV due to the relatively small surface area and the poor electron transfer. For P*p*PD modified electrode, the current densities of the anodic and cathodic peaks were increased and ΔE_p value was decreased to 500 mV compared to bare CPE, indicating that the P*p*PD film improved the conductivity of the electrode surface [44]. In the case of CNF modified electrode, the current density was increased significantly by about 60 % than that of the bare CPE, and the ΔE_p value was reduced to 250 mV. The manifested behaviour could be attributed to the high surface area and the high electrical properties of CNFs, which promote the electron transfer on the electrode surface. After modification of CPE surface by CNF/P*p*PD nanocomposite, an obvious increase in the current density of the redox peak was observed by about 115 % compared to the bare CPE, and sharp decrease in ΔE_p value was noticed, indicating a positive synergistic effect between CNFs and P*p*PD which increases the surface area and enhances the electron transfer at the electrode surface [38]. In addition when copper dendrites were electrodeposited on the surface of CNF/P*p*PD modified electrode, a well-defined redox peak was observed with a higher current density (about 240 % larger than that of bare CPE), illustrating that CuDs increases the surface area and catalyzes the redox reaction of $Fe(CN)_6^{3-}/Fe(CN)_6^{4-}$, moreover, the high conductivity of $Cu(OH)_2$ might further accelerate the electron transfer, despite the low conductivity of Cu_2O [26]. Furthermore, the electrochemical active surface areas (EASA) were estimated by Randles-Sevcik equation (**Eq. 1**) for different electrodes, which assumes mass transport by only diffusion process [57,58]:

$$i_p = 2.69 \times 10^5 \, n^{3/2} \, A \, D^{1/2} \, C \, v^{1/2} \qquad (\mathbf{Eq.\ 1})$$

where i_p is the peak current (A); n is the electron transfer number (n=1), A is the electroactive surface area (cm^2), D is the diffusion coefficient (6.7×10^{-6} $cm^2.s^{-1}$) [59], C is the concentration ($mol.cm^{-3}$), and v is the san rate ($V.s^{-1}$). The electroactive surface area of bare CPE, CPE-P*p*PD, CPE-CNF, CPE-CNF/P*p*PD, and CPE/CNF/P*p*PD/CuDs was calculated to be 0.05, 0.07, 0.09, 0.12, and 0.19 cm^2, respectively. To confirm these results, electrochemical impedance spectroscopy (EIS) measurements were performed in the same solution at 0.4 V *vs.* SCE with a small amplitude of 10 mV. The Nyquist plots are reported in **Fig. 6. (b)**.

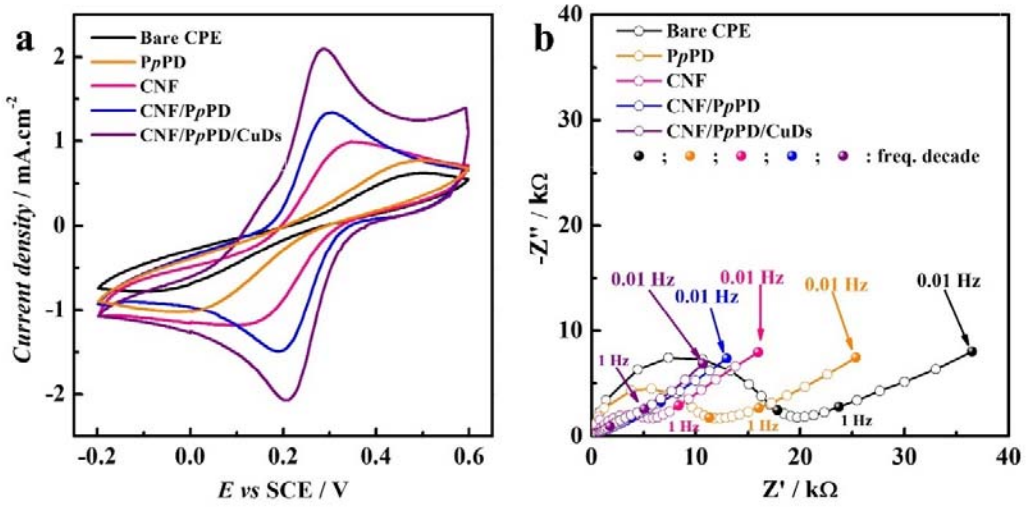

Fig. 6. *Cyclic voltammograms at a scan rate of v=50 mV s^{-1} (a) and EIS spectra measured at E=0.4 V vs SCE, with amplitude of 10 mV (b) of bare CPE, P*p*PD, CNF, CNF-P*p*PD, and CNF/P*p*PD/CuDs electrodes in 0.1 M KCl solution containing 5 mM of* $Fe(CN)_6^{3-}/Fe(CN)_6^{4-}$.

The CPE substrate presents a large semicircle in the region of high to low frequency, followed by a sloped line at low frequency. The electropolymerization of P*p*PD thin film on the CPE surface reduces the electron transfer resistance (R_{ct}) from 20 kΩ to 12 kΩ. These values are obtained from

an extrapolation of the high frequency loop to the real axis of the diagram. Indeed, the presence of P*p*PD thin film increases the electron transfer at the electrode surface by improving the electronic properties. The CPE substrate contains the non-conductive paraffin oil which reduces the active surface area and then, the electron transfer capability. The deposition of CNFs on CPE decreased the R_{ct} to 7 k**Ω**, owing to its good electronic properties and high surface area. In the case of CNF/P*p*PD and CNF/P*p*PD/CuDs modified electrodes, the R_{ct} is significantly lower as compared to that of CNF, P*p*PD and bare CPE electrodes. According to these results, the electropolymerization of P*p*PD on CNFs can generate a synergistic effect and presents enhanced electrical properties, which leads to the promotion of the electron transfer at the electrode. In addition, the incorporation of copper dendrites on CNF/P*p*PD offers a large number of active sites which could catalyse the reaction at the electrode surface. The EIS results are in good agreement with the CV results reported in **Fig. 6. (c)**.

3.4. Electrocatalytic performances of the prepared nanocomposites for methanol oxidation reaction

The catalytic performance of different nanocomposites was evaluated using CV and chronoamperometry techniques. **Fig. 7. (a)** reports the CV curves of CNF/P*p*PD/CuDs catalyst in 0.1 M NaOH solution with and without addition of methanol (1.5 M). In the presence of MeOH the voltammogram shows a large anodic peak around 0.9 V vs. SCE, indicating the electrooxidation of methanol at the electrode surface.

The catalytic effect of CNF/P*p*PD/CuDs on the electrooxidation of methanol was compared to that of CNF/CuDs and of P*p*PD/CuDs (**Fig. 7. (b)**). CNF/P*p*PD/CuDs displays superior catalytic activity

towards MOR with a current density of about 50 mA.cm^{-2}, while, CNF/CuDs and P*p*PD/CuDs exhibit 40 mA.cm^{-2} and 36 mA.cm^{-2}, respectively. The increased catalytic activity of CNF/P*p*PD/CuDs could be related to the good synergistic effect between CNF/P*p*PD support and the CuDs catalyst. CNFs present a high adsorption capability of methanol on the surface thanks to their high surface area, while P*p*PD presents a large number of amine groups on the surface, which play a significant role in increasing the catalytic performance of CuDs catalyst [48,60].

Concerning the mechanism of oxidation of methanol on copper-based catalyst, many reports stated that the CuOOH species play an important role in MOR [45,61]. In alkaline media, $Cu(OH)_2$ layer is converted to CuOOH by the entry of OH^- species at about 0.3 V according to ***Eq. 2*** [61]. Thereafter, methanol is oxidized on the active CuOOH layer and forms $Cu(OH)_2$ and CO_2 (***Eq. 3***), which causes a sharp increase in the current density [61,62].

$$Cu(OH)_2 + OH^- \leftrightarrow CuOOH + H_2O + e^- \quad (\boldsymbol{Eq.2})$$

$$CuOOH + CH_3OH + {}^5/_4\, O_2 \rightarrow Cu(OH)_2 + CO_2 + {}^3/_2\, H_2O \quad (\boldsymbol{Eq.3})$$

The effect of CuDs content on the electrocatalytic activity of CNF/P*p*PD/CuDs was studied using CV measurements. **Fig. SI.2** shows different CV curves in 0.1 M NaOH solution containing 1.5 M methanol with different CuDs amount, varied by adjusting the CuDs electrodeposition time. The electrocatalytic effect increases with the increase of the deposition time of CuDs until 45 s. However, a further increase of the deposition time resulted in decreasing the electrocatalytic effect of CuDs catalyst supported by CNF/P*p*PD. Normally, the increase of the CuDs content increases the catalytic sites on the surface, leading to an improvement of the catalytic performance. However, the excess of the CuDs negatively affects the performance of the catalyst by shortening the electron transfer path

[38,63]. Throughout this study, the optimal mass of CuDs obtained by a deposition time of 45 s was maintained.

The catalytic effect of CNF/P*p*PD/CuDs towards MOR was studied with a gradual increase of the concentration of methanol. **Fig. 7. (c)** shows the CV curves of CNF/P*p*PD/CuDs in 0.1 M NaOH solution with different methanol concentrations. The current density of the methanol oxidation peak increases with the increase of the methanol concentration until 3 M. In comparison with other reported catalysts [64–67], CNF/P*p*PD/CuDs shows a higher efficiency for MOR.

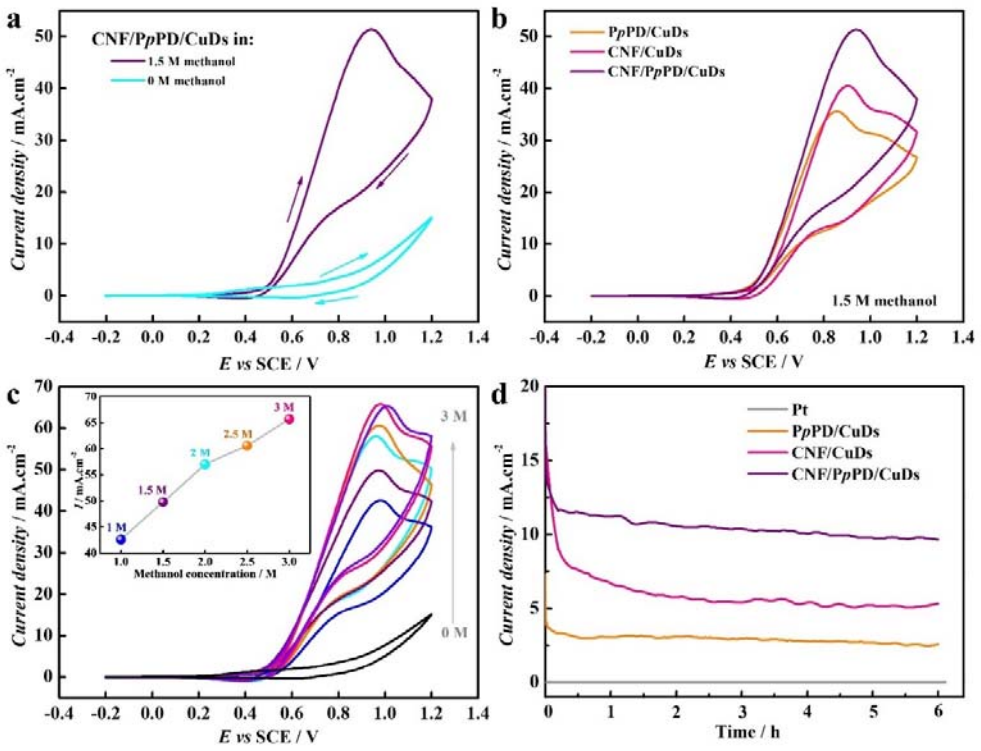

Fig. 7. *Cyclic voltammograms of CNF/PpPD/CuDs in 0.1 M NaOH solution with and without 1.5 M methanol (a), cyclic voltammograms of PpPD/CuDs, CNF/CuDs, and CNF/PpPD/CuDs in 0.1 M NaOH solution containing 1.5 M methanol (b), cyclic voltammograms of CNF/PpPD/CuDs in 0.1 M*

*NaOH solution with various concentrations of methanol, at a scan rate of ν=50 mV s^{-1} (c) and chronoamperograms of CNF/CuDs, P*p*PD/CuDs, CNF/P*p*PD/CuDs and Pt in 0.1 M NaOH solution containing 1.5 M of methanol at 0.9 V vs. SCE for 6 h (d).*

The long-term stability of the catalysts was evaluated by chronoamperometric measurements in 0.1 M NaOH solution containing 1.5 M methanol. **Fig. 7. (d)** shows the chronoamperometric curves of CNF/CuDs, P*p*PD/CuDs, CNF/P*p*PD/CuDs and Pt measured over 6 h. Comparing the responses of CuDs deposited on the individual CNF and P*p*PD supports, P*p*PD/CuDs showed a better stability during 6 h, confirming that P*p*PD improves the stability of the CuDs. It is due to the appropriate coordination with the amine groups as already indicated [39], while, CNF/CuDs presents a high current density, which could be explained by the high surface area and the good electrical properties of the CNFs [34,45]. In the case of CuDs supported on the hybrid CNF/P*p*PD nanocomposite, the current density is much higher than that of CNF/CuDs, P*p*PD/CuDs, and Pt, presenting a good stability over 6 h, indicating that the combination of CNF and P*p*PD as support for CuDs creates a good synergistic effect leading to a further improvement of the activity, stability, and durability of the CuDs. The chronoamperometry results are in good agreement with the CV results reported in **Fig. 7. (b)**. In order to highlight the catalytic performance of the prepared catalyst material with respect to previous works on similar material combinations and commercial catalyst, the catalytic activity of the prepared catalyst toward MOR was compared with that of other materials previously reported in the literature **(Table SI.3)**. It is important to point out that our catalyst shows an improved catalytic activity compared to that of other previous reported catalysts based on expensive or inexpensive metals, and of commercial catalyst. Moreover, our catalyst presents a remarkable stability toward MOR, and was tested for 6 h to provide a concrete information about the long-term

stability (**Fig. 7. (d)**). While, the stability of the catalyst reported in **Table SI.3**, was tested for less than 2 h. It is also noteworthy that the CNF/P*p*PD/CuDs was prepared by a rapid and simple way.

4. CONCLUSIONS

In this study, a new, inexpensive, and highly-efficient catalyst for methanol electrooxidation based on CuDs supported on CNF/P*p*PD, prepared by a simple and rapid process, was explored. P*p*PD was electropolymerized on a CNF modified electrode using CV. Then, the CuDs were electrodeposited at a constant potential. Various spectroscopic and microscopic techniques such as MEB, TEM, EDX, XRD and XPS were used to characterize the structure and the morphology of the prepared nanocomposites. The results show that the nanocomposite was successfully prepared and a three-dimensional dendritic structure consisting of Cu_2O and $Cu(OH)_2$ formed on the CNF/P*p*PD support. The electrochemical characterization by CV and EIS suggested that the CNF/P*p*PD/CuDs nanocomposite exhibited positive synergistic activity, which improved the electronic properties of the electrode compared to the individual components. The catalytic performance of the resulting catalyst for methanol electrooxidation was compared with that of P*p*PD/CuDs, CNF/CuDs, and Pt using CV and chronoamperometry in alkaline medium. The CNF/P*p*PD/CuDs catalyst showed higher catalytic activity and a good stability over 6 hours. This catalyst material is highly promising and can be a good alternative to the noble metal-based catalysts and contribute to the development of DMFC operating in alkaline media. Furthermore, it demonstrates the potential uses of hybrid carbon material/conducting polymer nanocomposite support for metal catalysts.

ACKNOWLEDGEMENTS

This work was supported by MESRSFC (*Ministère de l'Enseignement Supérieur et de la Recherche Scientifique et de la Formation des Cadres*) and CNRST (*Centre National pour la Recherche Scientifique et Technique*) (Project number PPR/2015/72). The authors thank Mrs. Stéphanie Delbrel and Mrs. Françoise Pillier for FEG-SEM analysis, Mrs. Sandra Casale for TEM measurements, and Mr. Cyrille Bazin for XRD analysis. We also appreciate the Erasmus + Program.

REFERENCES

[1] X. Wang, K. Wei, S. Yan, Y. Wu, J. Kang, P. Feng, S. Wang, F. Zhou, Y. Ling, Efficient and stable conversion of oxygen-bearing low-concentration coal mine methane by the electrochemical catalysis of SOFC anode: From pollutant to clean energy, Appl. Catal. B Environ. (2019) 118413. https://doi.org/10.1016/j.apcatb.2019.118413.

[2] G. Fu, J.-M. Lee, Ternary metal sulfides for electrocatalytic energy conversion, J. Mater. Chem. A. 7 (2019) 9386–9405. https://doi.org/10.1039/C9TA01438A.

[3] S.D. Tilley, Recent Advances and Emerging Trends in Photo-Electrochemical Solar Energy Conversion, Adv. Energy Mater. 9 (2019) 1802877. https://doi.org/10.1002/aenm.201802877.

[4] M. Aune, Å.L. Godbolt, K.H. Sørensen, M. Ryghaug, H. Karlstrøm, R. Næss, Concerned consumption. Global warming changing household domestication of energy, Energy Policy. 98 (2016) 290–297. https://doi.org/10.1016/j.enpol.2016.09.001.

[5] J. Nowotny, J. Dodson, S. Fiechter, T.M. Gür, B. Kennedy, W. Macyk, T. Bak, W. Sigmund, M. Yamawaki, K.A. Rahman, Towards global sustainability: Education on environmentally clean energy technologies, Renew. Sustain. Energy Rev. 81 (2018) 2541–2551. https://doi.org/10.1016/j.rser.2017.06.060.

[6] D.M. Fadzillah, S.K. Kamarudin, M.A. Zainoodin, M.S. Masdar, Critical challenges in the system development of direct alcohol fuel cells as portable power supplies: An overview, Int. J. Hydrog. Energy. 44 (2019) 3031–3054. https://doi.org/10.1016/j.ijhydene.2018.11.089.

[7] R. Rath, P. Kumar, S. Mohanty, S.K. Nayak, Recent advances, unsolved deficiencies, and future perspectives of hydrogen fuel cells in transportation and portable sectors, Int. J. Energy Res. 43 (2019) 8931–8955. https://doi.org/10.1002/er.4795.

[8] J. Prabhuram, R. Manoharan, Investigation of methanol oxidation on unsupported platinum electrodes in strong alkali and strong acid, J. Power Sources. 74 (1998) 54–61. https://doi.org/10.1016/S0378-7753(98)00012-3.

[9] S.M. Alia, G. Zhang, D. Kisailus, D. Li, S. Gu, K. Jensen, Y. Yan, Porous Platinum Nanotubes for Oxygen Reduction and Methanol Oxidation Reactions, Adv. Funct. Mater. 20 (2010) 3742–3746. https://doi.org/10.1002/adfm.201001035.

[10] S. Sharma, A. Ganguly, P. Papakonstantinou, X. Miao, M. Li, J.L. Hutchison, M. Delichatsios, S. Ukleja, Rapid Microwave Synthesis of CO Tolerant Reduced Graphene Oxide-Supported Platinum Electrocatalysts for Oxidation of Methanol, J. Phys. Chem. C. 114 (2010) 19459–19466. https://doi.org/10.1021/jp107872z.

[11] Y.C. Liu, X.P. Qiu, Y.Q. Huang, W.T. Zhu, Methanol electro-oxidation on mesocarbon microbead supported Pt catalysts, Carbon. 40 (2002) 2375–2380. https://doi.org/10.1016/S0008-6223(02)00115-X.

[12] I.S. Pieta, A. Rathi, P. Pieta, R. Nowakowski, M. Hołdynski, M. Pisarek, A. Kaminska, M.B. Gawande, R. Zboril, Electrocatalytic methanol oxidation over Cu, Ni and bimetallic Cu-Ni nanoparticles

supported on graphitic carbon nitride, Appl. Catal. B Environ. 244 (2019) 272–283. https://doi.org/10.1016/j.apcatb.2018.10.072.
[13] M.B. Gawande, A. Goswami, F.-X. Felpin, T. Asefa, X. Huang, R. Silva, X. Zou, R. Zboril, R.S. Varma, Cu and Cu-Based Nanoparticles: Synthesis and Applications in Catalysis, Chem. Rev. 116 (2016) 3722–3811. https://doi.org/10.1021/acs.chemrev.5b00482.
[14] P. Pattanayak, N. Pramanik, P. Kumar, P.P. Kundu, Fabrication of cost-effective non-noble metal supported on conducting polymer composite such as copper/polypyrrole graphene oxide (Cu 2 O/PPy–GO) as an anode catalyst for methanol oxidation in DMFC, Int. J. Hydrog. Energy. 43 (2018) 11505–11519. https://doi.org/10.1016/j.ijhydene.2017.04.300.
[15] D.C. Sesu, P. Marbaniang, S. Ingavale, A.C. Manohar, B. Kakade, Bi-Co-Cu Metal Oxide Foam as Significant Electrocatalyst for Methanol Electrooxidation, ChemistrySelect. 5 (2020) 306–311. https://doi.org/10.1002/slct.201904127.
[16] L. Han, P. Cui, H. He, H. Liu, Z. Peng, J. Yang, A seed-mediated approach to the morphology-controlled synthesis of bimetallic copper–platinum alloy nanoparticles with enhanced electrocatalytic performance for the methanol oxidation reaction, J. Power Sources. 286 (2015) 488–494. https://doi.org/10.1016/j.jpowsour.2015.04.003.
[17] I. Mintsouli, J. Georgieva, S. Armyanov, E. Valova, G. Avdeev, A. Hubin, O. Steenhaut, J. Dille, D. Tsiplakides, S. Balomenou, S. Sotiropoulos, Pt-Cu electrocatalysts for methanol oxidation prepared by partial galvanic replacement of Cu/carbon powder precursors, Appl. Catal. B Environ. 136–137 (2013) 160–167. https://doi.org/10.1016/j.apcatb.2013.01.059.
[18] B. Zhang, G. Yang, C. Li, K. Huang, J. Wu, S. Hao, Y. Huang, Electrochemical behaviors of hierarchical copper nano-dendrites in alkaline media, Nano Res. 11 (2018) 4225–4231. https://doi.org/10.1007/s12274-018-2010-3.
[19] A. Roy, H.S. Jadhav, M. Cho, J.G. Seo, Electrochemical deposition of self-supported bifunctional copper oxide electrocatalyst for methanol oxidation and oxygen evolution reaction, J. Ind. Eng. Chem. 76 (2019) 515–523. https://doi.org/10.1016/j.jiec.2019.04.019.
[20] J.N. Heo, J. Kim, J.Y. Do, N.-K. Park, M. Kang, Self-assembled electron-rich interface in defected ZnO:rGO-Cu:Cu2O, and effective visible light-induced carbon dioxide photoreduction, Appl. Catal. B Environ. 266 (2020) 118648. https://doi.org/10.1016/j.apcatb.2020.118648.
[21] J. Hwang, K.Y. Lee, Phase-transformation of hexagonal Cu2S microplates to nanoparticle-confined Cu2O microplates at low temperatures and their electro-catalytic property for methanol oxidation, Chem. Phys. 530 (2020) 110602. https://doi.org/10.1016/j.chemphys.2019.110602.
[22] A. El Attar, L. Oularbi, S. Chemchoub, M. El Rhazi, Preparation and characterization of copper oxide particles/polypyrrole (Cu2O/PPy) via electrochemical method: Application in direct ethanol fuel cell, Int. J. Hydrog. Energy. 45 (2020) 8887–8898. https://doi.org/10.1016/j.ijhydene.2020.01.008.
[23] H. Ashassi-Sorkhabi, B. Rezaei-Moghadam, E. Asghari, Electrosynthesis of polypyrrole–nanodiamond composite film under ultrasound irradiation: Promotion for methanol electrooxidation by gold and Cu2O nanostructures, J. Taiwan Inst. Chem. Eng. 75 (2017) 263–270. https://doi.org/10.1016/j.jtice.2017.03.011.
[24] F. Baştürk, H. Yüksel, R. Solmaz, Fabrication of three-dimensional copper nanodomes as anode materials for direct methanol fuel cells, Int. J. Hydrog. Energy. 44 (2019) 14235–14242. https://doi.org/10.1016/j.ijhydene.2019.02.137.
[25] G. Chen, Y. Pan, T. Lu, N. Wang, X. Li, Highly catalytical performance of nanoporous copper for electro-oxidation of methanol in alkaline media, Mater. Chem. Phys. 218 (2018) 108–115. https://doi.org/10.1016/j.matchemphys.2018.07.034.
[26] S.M. Pawar, B.S. Pawar, A.I. Inamdar, J. Kim, Y. Jo, S. Cho, S.S. Mali, C.K. Hong, J. Kwak, H. Kim, H. Im, In-situ synthesis of Cu(OH)2 and CuO nanowire electrocatalysts for methanol electro-oxidation, Mater. Lett. 187 (2017) 60–63. https://doi.org/10.1016/j.matlet.2016.10.079.

[27] R. Chang, L. Zheng, C. Wang, D. Yang, G. Zhang, S. Sun, Synthesis of hierarchical platinum-palladium-copper nanodendrites for efficient methanol oxidation, Appl. Catal. B Environ. 211 (2017) 205–211. https://doi.org/10.1016/j.apcatb.2017.04.040.
[28] L. Osmieri, R. Escudero-Cid, M. Armandi, A.H.A. Monteverde Videla, J.L. García Fierro, P. Ocón, S. Specchia, Fe-N/C catalysts for oxygen reduction reaction supported on different carbonaceous materials. Performance in acidic and alkaline direct alcohol fuel cells, Appl. Catal. B Environ. 205 (2017) 637–653. https://doi.org/10.1016/j.apcatb.2017.01.003.
[29] E. Antolini, Composite materials: An emerging class of fuel cell catalyst supports, Appl. Catal. B Environ. 100 (2010) 413–426. https://doi.org/10.1016/j.apcatb.2010.08.025.
[30] S. Sharma, B.G. Pollet, Support materials for PEMFC and DMFC electrocatalysts—A review, J. Power Sources. 208 (2012) 96–119. https://doi.org/10.1016/j.jpowsour.2012.02.011.
[31] A. Shahzeydi, M. Ghiaci, L. Jameie, M. Panjepour, Immobilization of N-doped carbon porous networks containing copper nanoparticles on carbon felt fibers for catalytic applications, Appl. Surf. Sci. 485 (2019) 194–203. https://doi.org/10.1016/j.apsusc.2019.04.205.
[32] W. Xu, D. Du, R. Lan, J. Humphreys, D.N. Miller, M. Walker, Z. Wu, J.T.S. Irvine, S. Tao, Electrodeposited NiCu bimetal on carbon paper as stable non-noble anode for efficient electrooxidation of ammonia, Appl. Catal. B Environ. 237 (2018) 1101–1109. https://doi.org/10.1016/j.apcatb.2016.11.003.
[33] J.C. Calderón, G. García, L. Calvillo, J.L. Rodríguez, M.J. Lázaro, E. Pastor, Electrochemical oxidation of CO and methanol on Pt–Ru catalysts supported on carbon nanofibers: the influence of synthesis method, Appl. Catal. B Environ. 165 (2015) 676–686. https://doi.org/10.1016/j.apcatb.2014.10.077.
[34] X. Mu, Z. Xu, Y. Ma, Y. Xie, H. Mi, J. Ma, Graphene-carbon nanofiber hybrid supported Pt nanoparticles with enhanced catalytic performance for methanol oxidation and oxygen reduction, Electrochimica Acta. 253 (2017) 171–177. https://doi.org/10.1016/j.electacta.2017.09.029.
[35] R. Arukula, M. Vinothkannan, A.R. Kim, D.J. Yoo, Cumulative effect of bimetallic alloy, conductive polymer and graphene toward electrooxidation of methanol: An efficient anode catalyst for direct methanol fuel cells, J. Alloys Compd. 771 (2019) 477–488. https://doi.org/10.1016/j.jallcom.2018.08.303.
[36] M. Eswaran, R. Dhanusuraman, P.-C. Tsai, V.K. Ponnusamy, One-step preparation of graphitic carbon nitride/Polyaniline/Palladium nanoparticles based nanohybrid composite modified electrode for efficient methanol electro-oxidation, Fuel. 251 (2019) 91–97. https://doi.org/10.1016/j.fuel.2019.04.040.
[37] E. Morsbach, S. Kunz, M. Bäumer, Novel nanoparticle catalysts for catalytic gas sensing, Catal. Sci. Technol. 6 (2016) 339–348. https://doi.org/10.1039/C5CY01553G.
[38] E.M. Halim, M. Elbasri, H. Perrot, O. Sel, K. Lafdi, M. El Rhazi, Synthesis of carbon nanofibers/poly(para-phenylenediamine)/nickel particles nanocomposite for enhanced methanol electrooxidation, Int. J. Hydrog. Energy. 44 (2019) 24534–24545. https://doi.org/10.1016/j.ijhydene.2019.07.141.
[39] B. Wu, J. Zhu, X. Li, X. Wang, J. Chu, S. Xiong, PtRu nanoparticles supported on p-phenylenediamine-functionalized multiwalled carbon nanotubes: enhanced activity and stability for methanol oxidation, Ionics. 25 (2019) 181–189. https://doi.org/10.1007/s11581-018-2590-7.
[40] Y. Zhao, R. Fan, Z. Chen, Q. Zhao, J. Li, L. Yang, J. Xue, Engineering beneficial structures and morphologies of M-N-C oxygen-reduction catalysts derived from different metal-containing precursors, Ionics. 24 (2018) 1733–1744. https://doi.org/10.1007/s11581-017-2346-9.
[41] D.A. Shirley, High-Resolution X-Ray Photoemission Spectrum of the Valence Bands of Gold, Phys. Rev. B. 5 (1972) 4709–4714. https://doi.org/10.1103/PhysRevB.5.4709.

[42] M.D. Brown, M.H. Schoenfisch, Nitric Oxide Permselectivity in Electropolymerized Films for Sensing Applications, ACS Sens. 1 (2016) 1453–1461. https://doi.org/10.1021/acssensors.6b00596.
[43] I. Adraoui, M. El Rhazi, A. Amine, L. Idrissi, A. Curulli, G. Palleschi, Lead Determination by Anodic Stripping Voltammetry Using a p-Phenylenediamine Modified Carbon Paste Electrode, Electroanalysis. 17 (2005) 685–693. https://doi.org/10.1002/elan.200403140.
[44] F.E. Salih, L. Oularbi, E. Halim, M. Elbasri, A. Ouarzane, M. El Rhazi, Conducting Polymer/Ionic Liquid Composite Modified Carbon Paste Electrode for the Determination of Carbaryl in Real Samples, Electroanalysis. 30 (2018) 1855–1864. https://doi.org/10.1002/elan.201800152.
[45] N.A. Barakat, M. El-Newehy, S.S. Al-Deyab, H.Y. Kim, Cobalt/copper-decorated carbon nanofibers as novel non-precious electrocatalyst for methanol electrooxidation, Nanoscale Res. Lett. 9 (2014) 2. https://doi.org/10.1186/1556-276X-9-2.
[46] H. Rahal, R. Kihal, A.M. Affoune, S. Rahal, Electrodeposition and characterization of Cu2O thin films using sodium thiosulfate as an additive for photovoltaic solar cells, Chin. J. Chem. Eng. 26 (2018) 421–427. https://doi.org/10.1016/j.cjche.2017.06.023.
[47] S. Laidoudi, A.Y. Bioud, A. Azizi, G. Schmerber, J. Bartringer, S. Barre, A. Dinia, Growth and characterization of electrodeposited Cu2O thin films, Semicond. Sci. Technol. 28 (2013) 115005. https://doi.org/10.1088/0268-1242/28/11/115005.
[48] S. Masuda, K. Mori, Y. Futamura, H. Yamashita, PdAg Nanoparticles Supported on Functionalized Mesoporous Carbon: Promotional Effect of Surface Amine Groups in Reversible Hydrogen Delivery/Storage Mediated by Formic Acid/CO2, ACS Catal. 8 (2018) 2277–2285.
[49] A. Frattini, N. Pellegri, D. Nicastro, O. de Sanctis, Effect of amine groups in the synthesis of Ag nanoparticles using aminosilanes, Mater. Chem. Phys. 94 (2005) 148–152. https://doi.org/10.1016/j.matchemphys.2005.04.023.
[50] M. Celebi, M. Yurderi, A. Bulut, M. Kaya, M. Zahmakiran, Palladium nanoparticles supported on amine-functionalized SiO2 for the catalytic hexavalent chromium reduction, Appl. Catal. B Environ. 180 (2016) 53–64. https://doi.org/10.1016/j.apcatb.2015.06.020.
[51] Y. Karatas, A. Bulut, M. Yurderi, I.E. Ertas, O. Alal, M. Gulcan, M. Celebi, H. Kivrak, M. Kaya, M. Zahmakiran, PdAu-MnOx nanoparticles supported on amine-functionalized SiO2 for the room temperature dehydrogenation of formic acid in the absence of additives, Appl. Catal. B Environ. 180 (2016) 586–595. https://doi.org/10.1016/j.apcatb.2015.06.060.
[52] S. Shahrokhian, E.K. Sanati, H. Hosseini, Advanced on-site glucose sensing platform based on a new architecture of free-standing hollow Cu(OH)2 nanotubes decorated with CoNi-LDH nanosheets on graphite screen-printed electrode, Nanoscale. 11 (2019) 12655–12671. https://doi.org/10.1039/C9NR02720C.
[53] Y. Wu, M. Song, Q. Wang, T. Wang, X. Wang, A highly selective conversion of toxic nitrobenzene to nontoxic aminobenzene by Cu2O/Bi/Bi2MoO6, Dalton Trans. 47 (2018) 8794–8800. https://doi.org/10.1039/C8DT01536H.
[54] Z. Zhang, P. Wang, Highly stable copper oxide composite as an effective photocathode for water splitting via a facile electrochemical synthesis strategy, J. Mater. Chem. 22 (2012) 2456–2464. https://doi.org/10.1039/C1JM14478B.
[55] M. Yin, C.-K. Wu, Y. Lou, C. Burda, J.T. Koberstein, Y. Zhu, S. O'Brien, Copper Oxide Nanocrystals, J. Am. Chem. Soc. 127 (2005) 9506–9511. https://doi.org/10.1021/ja050006u.
[56] L.P. Kazansky, Y.E. Pronin, I.A. Arkhipushkin, XPS study of adsorption of 2-mercaptobenzothiazole on a brass surface, Corros. Sci. 89 (2014) 21–29. https://doi.org/10.1016/j.corsci.2014.07.055.
[57] S. Abbas, H. Lee, J. Hwang, A. Mehmood, H.-J. Shin, S. Mehboob, J.-Y. Lee, H.Y. Ha, A novel approach for forming carbon nanorods on the surface of carbon felt electrode by catalytic etching for high-performance vanadium redox flow battery, Carbon. 128 (2018) 31–37. https://doi.org/10.1016/j.carbon.2017.11.066.

[58] J. Lu, I. Do, L.T. Drzal, R.M. Worden, I. Lee, Nanometal-Decorated Exfoliated Graphite Nanoplatelet Based Glucose Biosensors with High Sensitivity and Fast Response, ACS Nano. 2 (2008) 1825–1832. https://doi.org/10.1021/nn800244k.
[59] S.J. Konopka, B. McDuffie, Diffusion coefficients of ferri- and ferrocyanide ions in aqueous media, using twin-electrode thin-layer electrochemistry, (2002). https://doi.org/10.1021/ac50160a042.
[60] I.S. Pieta, A. Rathi, P. Pieta, R. Nowakowski, M. Hołdynski, M. Pisarek, A. Kaminska, M.B. Gawande, R. Zboril, Electrocatalytic methanol oxidation over Cu, Ni and bimetallic Cu-Ni nanoparticles supported on graphitic carbon nitride, Appl. Catal. B Environ. 244 (2019) 272–283. https://doi.org/10.1016/j.apcatb.2018.10.072.
[61] S.M. Pawar, J. Kim, A.I. Inamdar, H. Woo, Y. Jo, B.S. Pawar, S. Cho, H. Kim, H. Im, Multi-functional reactively-sputtered copper oxide electrodes for supercapacitor and electro-catalyst in direct methanol fuel cell applications, Sci. Rep. 6 (2016) 21310. https://doi.org/10.1038/srep21310.
[62] A.P. Periasamy, J. Liu, H.-M. Lin, H.-T. Chang, Synthesis of copper nanowire decorated reduced graphene oxide for electro-oxidation of methanol, J. Mater. Chem. A. 1 (2013) 5973–5981. https://doi.org/10.1039/C3TA10745K.
[63] H. Zhu, J. Wang, X. Liu, X. Zhu, Three-dimensional porous graphene supported Ni nanoparticles with enhanced catalytic performance for Methanol electrooxidation, Int. J. Hydrog. Energy. 42 (2017) 11206–11214. https://doi.org/10.1016/j.ijhydene.2017.02.189.
[64] P. Pattanayak, N. Pramanik, P. Kumar, P.P. Kundu, Fabrication of cost-effective non-noble metal supported on conducting polymer composite such as copper/polypyrrole graphene oxide (Cu2O/PPy–GO) as an anode catalyst for methanol oxidation in DMFC, Int. J. Hydrog. Energy. 43 (2018) 11505–11519. https://doi.org/10.1016/j.ijhydene.2017.04.300.
[65] L. Tao, S. Dou, Z. Ma, A. Shen, S. Wang, Simultaneous Pt deposition and nitrogen doping of graphene as efficient and durable electrocatalysts for methanol oxidation, Int. J. Hydrog. Energy. 40 (2015) 14371–14377. https://doi.org/10.1016/j.ijhydene.2015.02.104.
[66] Y. Haldorai, D. Arreaga-Salas, C.S. Rak, Y.S. Huh, Y.-K. Han, W. Voit, Platinized titanium nitride/graphene ternary hybrids for direct methanol fuel cells and titanium nitride/graphene composites for high performance supercapacitors, Electrochimica Acta. 220 (2016) 465–474. https://doi.org/10.1016/j.electacta.2016.10.130.
[67] M. Zhang, J. Xie, Q. Sun, Z. Yan, M. Chen, J. Jing, Enhanced electrocatalytic activity of high Pt-loadings on surface functionalized graphene nanosheets for methanol oxidation, Int. J. Hydrog. Energy. 38 (2013) 16402–16409. https://doi.org/10.1016/j.ijhydene.2013.09.108.